Integrated Navigation and Sense & Avoid Systems for Micro Aerial Vehicles

P. Vörsmann, S. Winkler, J.-B. Park

Institute of Aerospace Systems, TU Braunschweig, Germany (E-mail: p.voersmann@tu-bs.de)

Abstract

The paper deals with integrated navigation and sense & avoid systems for small unmanned aerial vehicles (UAV). First an introduction to the current UAV activities of the institute is given. It is followed by an overview about the integrated navigation system developed for small UAVs. The system is based on a tightly-coupled GPS/INS architecture. But instead of using delta-ranges, time-differenced carrier phases are used to aid the INS. Finally, results from navigation filter validation in flight tests are presented. After that an overview about sense and avoid strategies for application in small unmanned aircraft is given. From this a guideline for developing such a system for the institute's UAVs is presented.

Keywords: UAV, MAV, integrated navigation, sense & avoid

1. Introduction

Micro Aerial Vehicles (MAVs) are a major field of research at the Institute of Aerospace Systems (ILR) of the Technical University of Braunschweig, Germany. Currently, the institute is involved in two MAV projects. First, the ILR is the leader of the university's MAV project CAROLO (initiated in 2001). And second, it is the leader of the project AutoMAV within the German National Aerospace Program 2003-2007. Both projects are focused on fully autonomous flight. "Fully autonomous" in this context means that all flight control and navigation algorithms are running on the on-board computer of the aircraft. Hence, there is no continuous data link between ground station and aircraft necessary in order to enable autonomy.

The project AutoMAV (2004-2006) is being conducted by a team of the leading German MAV research institutions. The goal of the project is the development of a very agile, fully autonomous fixed-wing outdoor MAV for observing airports and other critical facilities in order to decrease the danger of terroristic acts (Figure 1). The current prototype has a wing span of 38 cm, a weight of about 400 g and is operating at a velocity of about 65 km/h for more than 30 min. A good flight performance of the automatically controlled aircraft is of primary importance and will exceed the performance of CAROLO P50 (Figure 2). This will be achieved by an integrated navigation system primarily consisting of satellite and inertial navigation components (GPS and INS). Besides a camera for live-video, the aircraft will be equipped with a rescue system for save operation.

The former MAV project CAROLO was initiated in 2001. The final MAV prototype is CAROLO P50 (Figure 2). It has a wing span of 50 cm, a weight of about 450 g and is operating at a velocity of about 70 km/h for more than 20 min. The highly-integrated flying robot is equipped with a video camera and provides live-video in the close-up range. The aircraft is flying fully autonomously via GPS waypoint navigation including take-off and landing.

Not only MAVs but in all five different unmanned aircraft have been developed, ranging from 40 cm to 330 cm wingspan. Four of the five aircraft fly fully autonomously from start to landing using waypoint navigation. For characteristics and possible applications of each aircraft see [19]. Current activities involve navigation system improvements and sense & avoid technology implementation on board. The paper summarizes current results and next activities.

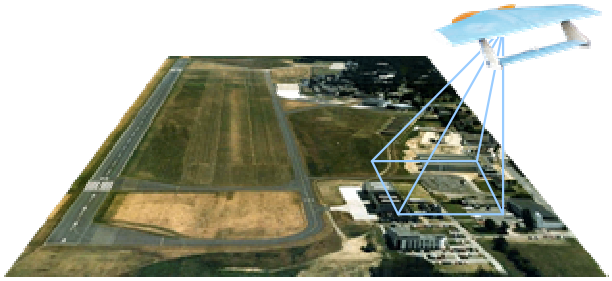

Figure 1: Airport surveillance by the AutoMAV.

Figure 2: MAV Carolo P50.

2. Integrated Navigation System

In general, in order to carry out sophisticated missions and to obtain a good flight performance of fully autonomous MAVs, a reliable navigation solution, especially of the attitude, is of significant importance. For this, an Inertial Measurement Unit (IMU) based on micro-electromechanical systems (MEMS) was tightly-coupled (usage of GPS raw data) with a single frequency stand-alone GPS receiver.

2.1 Sensor System

The Miniature Integrated Navigation & Control (MINC) System was developed at the Institute of Aerospace Systems and will be used for the AutoMAV. It consists of two modules, the TrIMU sensor block and the MINC Core navigational computer. The sensor block contains a MEMS-based 3-axis-IMU, pressure sensors for static and impact pressure and acts as a low-level I/O interface. Besides up to 12 servo actuators and a remote control receiver can be connected which allows for manual control of the aircraft during flight controller development and test. In addition, external A/D converters can be connected to increase analog input capabilities. The standard sensors and its measurement ranges are listed in Table 1.

Table 1: Technical data of the sensor system.

MEMS Sensors	Measurement range
angular rates (x, y, z)	±300°/s ≈ 5.2 rad/s
linear acceleration (x, y)	±1.5 g ≈ ±14.7 m/s²
linear acceleration (x, z)	±8 g ≈ ±78.5 m/s²
static pressure	15 to 105 kPa
impact pressure	0 to 1.250 Pa

All communication between TrIMU and MINC Core for sensor data and servo commands is done by means of data packets via a single bidirectional serial link. The MINC Core mainly consists of a powerful 32 bit RISC CPU with 16 MB RAM and 32 MB ROM. The CPU runs at approximately 200 MHz and offers, as a main feature of the MINC System, a hardware Floating Point Unit for floating point operations with single (32 bit) and double (64 bit) precision. This greatly simplifies the development and implementation of navigation and flight control algorithms, since even demanding algorithms can be directly implemented using floating point numbers.

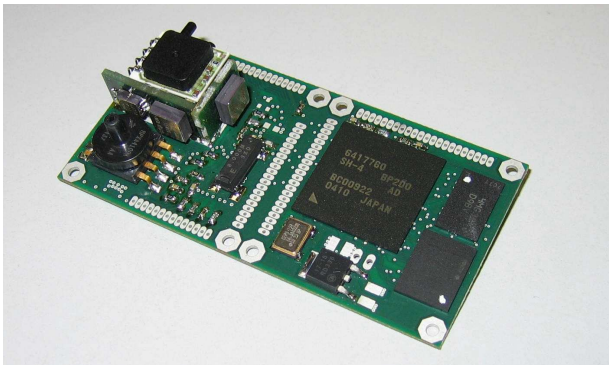

Figure 3: Miniature Integrated Navigation & Control System.

The whole MINC Systems, as shown in Figure 3, measures $40 \times 80 \times 15$ mm³ and weights only 20 g (w/o cables and connectors). Including GPS, the whole high performance autopilot system weights 45 g.

2.2 Navigation Filter

For GPS/INS integration a discrete error state Kalman Filter of state vector **x** was used [8]. By processing measurements from a single-antenna single-frequency stand-alone GPS receiver, it provides estimates for the three position, three velocity and three attitude errors as well as the three errors in the gyro sensor signal bias estimates, the three errors in the accelerometer signal bias estimates, the error in the GPS receiver (RX) clock error and the error in the GPS RX clock drift (17 states):

$$\mathbf{x} = \begin{bmatrix} \delta\mathbf{r} & \dots & \text{position error} \\ \delta\mathbf{v} & \dots & \text{velocity error} \\ \delta\boldsymbol{\varphi} & \dots & \text{attitude error} \\ \delta\boldsymbol{\omega} & \dots & \text{error of est. gyro signal bias} \\ \delta\mathbf{a} & \dots & \text{error of est. acc. signal bias} \\ \delta(c\,\Delta t) & \dots & \text{error of RX clock error} \\ \delta(c\,\Delta \dot{t}) & \dots & \text{error of RX clock drift} \end{bmatrix} \quad (1)$$

As aiding information, GPS raw data were used in order to closely meet the Kalman Filter requirement of zero-mean and uncorrelated white measurement noise (tightly-coupled). Furthermore, with such a filter the IMU can still be aided by GPS when there are less than 4 satellites in field-of-view (FOV) of the GPS antenna. These two significant features can not be fulfilled by using the position and velocity outputs of the GPS receiver directly (loosely-coupled).

Often, the measurement vector **z** of a tightly-coupled Kalman Filter contains ranges and delta-ranges. But in the developed filter the delta-ranges were replaced by time-differenced carrier phases. The key idea of this method is to improve the velocity aiding and hence the attitude estimate of the filter which is the most important aircraft state in order to achieve good flight performances of autonomous MAVs.

Based on the method used in [6,9], this method was adapted in [21] in order to process time-differenced carrier phase measurements of a stand-alone GPS receiver for land vehicles and in [22] it was used for MAV navigation. It was shown that the filter with time-differenced carrier phases achieves a better velocity and attitude accuracy than the filter using delta-ranges. The method allows to use precise carrier phase measurements without solving the integer ambiguities. Compared to the delayed state Kalman filter which would be commonly used in such a case this method does not induce additional cross-correlation between measurements at one epoch. Hence, the measurement noise covariance matrix **R** of the filter keeps its diagonal shape. This allows a sequential measurement processing without previous decorrelation and, hence, the avoidance of the matrix inversion in the Kalman gain computation. In the following a short summary of this method will be given. For more details one might refer to the references mentioned above.

A single carrier phase measurement at epoch t_k (subscript k) can be modeled as:

$$\left(\tilde{\varphi}_k + N\right)\lambda = \rho_k + c\,\Delta t_k + n_k \quad (2)$$

where φ is the carrier phase (measurement: ~), N the integer phase ambiguity, λ the carrier wavelength, ρ the distance between user antenna and GPS satellite (the range), $c\Delta t$ the receiver clock error in [m] and n the measurement noise. The time-differenced carrier phase measurement results in:

$$\begin{aligned} \left(\tilde{\varphi}_k - \tilde{\varphi}_{k-1}\right)\lambda &= \rho_k - \rho_{k-1} + c\,\Delta t_k - c\,\Delta t_{k-1} + n_k - n_{k-1} \\ &= \rho_k - \rho_{k-1} + c\,\Delta t_k - c\,\Delta t_{k-1} + n'_k\,. \end{aligned} \quad (4)$$

The noise term n'_k contains the remaining noise after time-differencing.

The measurement provided to the Kalman filter is the predicted (^) minus the measurement (~) time-differenced carrier phase:

$$h_k = \left(\hat{\tilde{\varphi}}_k - \hat{\tilde{\varphi}}_{k-1}\right)\lambda \quad - \quad \left(\tilde{\varphi}_k - \tilde{\varphi}_{k-1}\right)\lambda \tag{6}$$

After some calculations and simplifications, the linearized Kalman filter measurement equation for a single time-differenced carrier phase measurement results in:

$$z_k = \mathbf{H}_k\, \mathbf{x}_k + n'_k \tag{7}$$

where the measurement matrix $\mathbf{H}_k$ is:

$$\mathbf{H}_k = \left[\mathbf{H}_k^{\dagger} \left(\int_{t_{k-1}}^{t_k} \mathbf{\Phi}_{t,t_{k-1}}\, dt \right) \mathbf{\Phi}_{t_{k-1},t_k} + \mathbf{H}_k^{\#} \right] \mathbf{x} + n'_k \tag{8}$$

with

$$\mathbf{H}_k^{\dagger} = \left[\mathbf{0}^T \;\middle|\; -\mathbf{e}_{g,k}^T \;\middle|\; \mathbf{0}^T \;\middle|\; \mathbf{0}^T \;\middle|\; \mathbf{0}^T \;\middle|\; 0 \;\middle|\; 1 \right] \tag{9}$$

and

$$\mathbf{H}_k^{\#} = \left[\mathbf{0}^T \;\middle|\; \mathbf{0}^T \;\middle|\; \mathbf{e}_{g,k}^T \;\; \Delta\hat{\mathbf{l}}_{g,k}^{\times} \;\middle|\; \mathbf{e}_{g,k}^T \;\; \Delta T\, \hat{\mathbf{l}}_{g,k-1}^{\times}\, \hat{\mathbf{T}}_{gb,k} \;\middle|\; \mathbf{0}^T \;\middle|\; 0 \right] \tag{10}$$

In these equations subscript g denotes vectors in the geodetic frame, superscript $\times$ the cross-product matrix of the prefixed vector, $\mathbf{\Phi}_{2,1}$ the state transition matrix to go from time t_1 to time t_2, $\mathbf{e}$ the unity vector from user GPS antenna to GPS satellite, $\Delta\mathbf{l} = \mathbf{l}_k - \mathbf{l}_{k-1}$, ($\mathbf{l}$: vector from IMU to GPS antenna, lever arm) and $\mathbf{T}_{gb}$ the rotation matrix from body to geodetic frame. The geodetic frame is identical to the north-east-down frame.

2.3 Validation in Flight Test

A GN&C test platform was developed by the institute. It is a small UAV of 2 m wing span and about 5 kg maximum take-off weight. Due to 1.8 kg payload capacity, it can be equipped with different accurate navigation sensors for MEMS-based navigation system validation. For the flight test the GN&C test platform was equipped with both the reference navigation system described above and the MINC System.

In order to visualize the considered flight trajectory, the roll angle and the number of GPS satellites tracked is shown in Figure 4. It consists of lower and higher dynamic parts. Up to 40440 s the trajectory mainly consists of turns with large curve radii and roll angles of about 30°. After that, up to 40600 s, the curve radii were decreased which caused roll angles of about 60°. Between 40600 s and 40720 s a horizontal flight with alternating longitudinal acceleration and deceleration was carried out. After that a horizontal sinuous line was flown. During all periods the UAV was controlled via remote control from the pilot on the ground.

The accuracy of the low-cost navigation system is given with respect to the reference navigation system. The error of roll angle Φ, pitch angle Θ and yaw angle Ψ using the 17 state Kalman filter with state vector from Eq. (1) is shown in Figure 5. As expected, roll and pitch angle show a little better accuracy than yaw angle due to gravity influence.

Finally, a new Kalman filter with three more states was developed. The new states are the gyro drifts, because the 17 state filter has shown non-constant gyro biases. Reason is that the MEMS-IMU was not temperature calibrated but its gyros are subject to large temperature influences. The improvement when estimating the gyro drift in addition to the biases is shown as relative cumulative frequencies in Figure 6. It shows, for example, that now 75% of the absolute roll angle errors $|\delta\Phi|$ are smaller than 0.5° compared to 50% when using the 17 state filter. The results are summarized in Table 1.

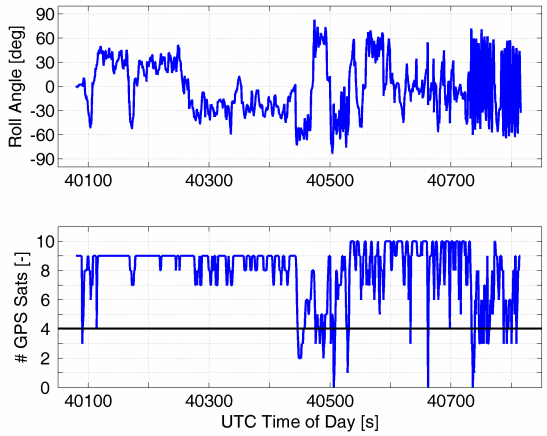

Figure 4: Roll angle and number of satellites tracked during flight test.

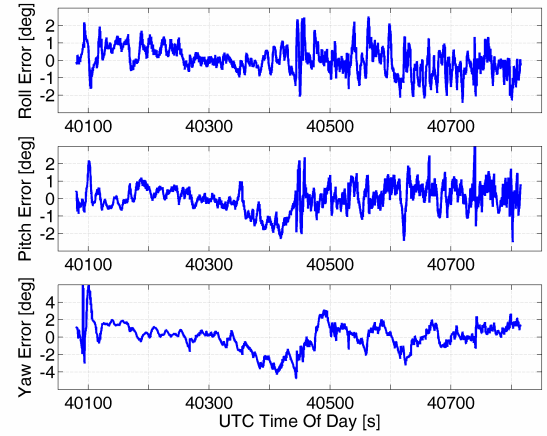

Figure 5: Attitude errors of the low-cost navigation system.

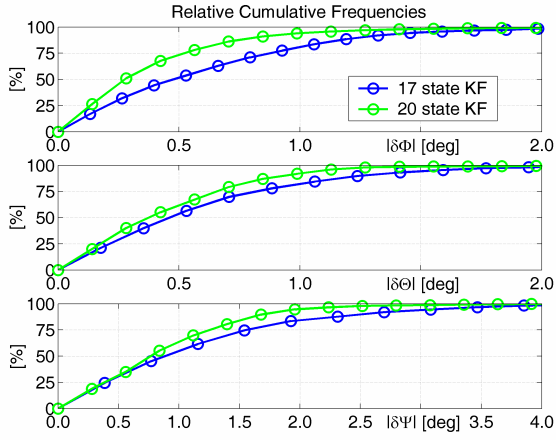

Figure 6: Comparison of relative cumulative frequency of attitude errors for different Kalman filters.

Table 1: Attitude errors of the MEMS-based GPS/INS system

Attitude Error (1σ)	17 state KF	20 state KF
Roll angle	0.76°	0.52°
Pitch angle	0.75°	0.58°
Yaw angle	1.50°	1.10°

3. Sense & Avoid System

The necessity of the research in "Sense and Avoid" consists of the implementation of appropriate systems into MAVs with the objective to enable the MAVs to detect obstacles and avoid them actively. The ability to sense obstacles and avoid these independently completes the autonomous flight. For these purposes, search algorithms which are actual subjects of research in robotics as well as in the UAV sector shall be developed and enhanced. The implementation of the algorithms for avoiding obstacles shall be investigated first by means of static obstacles and then be broadened to dynamic obstacles.

Therefore, the basis of this subject is the substantiated knowledge of *collision-free* path planning for mobile robots in their workspace. In this context, topological maps as roadmaps, potential field methods and kinodynamic methods can be implemented.

The potential field method assumes that the object – e.g. robot, UAV – underlies an artificial potential which consists of an attractive potential and repulsive potential. The attractive potential pulls the object toward the goal while the repulsive potential repels the object from the obstacles. The potential field method, however, shows problems dealing with local minimums.

In addition to the potential field method, the kinodynamic motion planning can be complementary applied by finding a collision-free path.

This section tries to give a basic insight into the topic of path planning for the implementation into an UAV system.

3.1 Path Planning

Path planning deals with the computation of control commands with which the change from initial configuration to the end configuration of a physical object can be achieved [12,13,14].

The inputs are geometric data of the object as well as that of the obstacles, kinematic and dynamic characteristic of the object and the initial and end configuration of the object.

Thereby, the transformation of the real workspace *W* into the abstract configuration space *C* is a requirement for the application of path planning methods. The configuration space is the set of all possible configurations *q* and includes the free space denoted by C_{free} and the obstacle space denoted by $C_{obstacle}$. Consequently, it is obvious that more configuration parameters are needed to represent the state proper with higher degree of freedom. For instance, for a MAV with six degrees of freedom the configuration parameter may be set as $q = (x, y, z, \Psi, \Theta, \Phi)$.

The principal advantage of this kind of representation is the transformation of a three dimensional moving object into a point in a modified obstacle space.

3.2 Potential Field Method

The main idea of the potential field method is that an artificial potential can be assigned to the environment in which the object – e.g. robot, UAV - is moving. This artificial potential $U(q)$ is differentiable and consists of an attractive potential $U_{att}(q)$ and a repulsive potential $U_{rep}(q)$. In this regard, the attractive potential is denoted to the goal and the repulsive potential to the obstacle respectively. The attractive potential increases with the distance to the goal. Contrary to this, the repulsive potential decreases with the distance to the obstacle. Thus the potentials show antithetic characteristics.

The differentiation of the potential function $U(q)$ results in a gradient $\nabla U(q)$ pointing in the direction of maximum increase of this potential function. Instead of following the maximum increase in the potential function, we attempt to move the object along the negated gradient $-\nabla U(q)$ of the potential function. Therefore, the UAV is leaded incrementally toward the goal by gradient descent.

A variety of approaches in building potential function such as *conic*, *parabolic* and a combination of the both for the attractive potential and *Gaussian distribution* for the repulsive potential are introduced in the literature [1,3,4,13].

With the definition of the distance between the goal configuration and other configurations, expressed in Eq. (11), the parabolic potential function for $U_{att}(q)$ can be stated as in Eq. (12),

$$\rho_{goal}(q) = \left\| q - q_{goal} \right\| \tag{11}$$

$$U_{att}(q) = \frac{1}{2}\xi\rho_{goal}^2(q) \tag{12}$$

Therefore, the negated gradient of this potential can be derived,

$$-\nabla U_{att}(q) = -\xi\left(q - q_{goal}\right) \tag{13}$$

For example, a parabolic attractive potential function is shown in Figure 6.

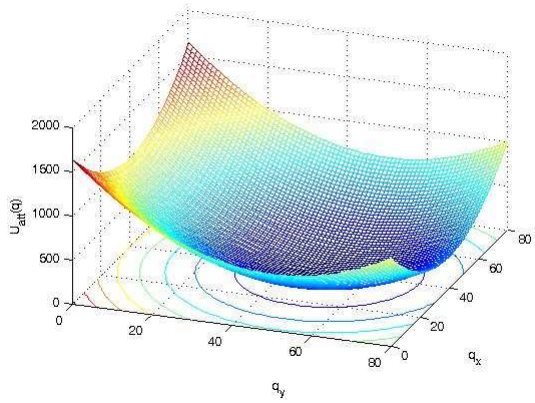

Figure 6 Attractive potential function $U_{att}(q)$

The repulsive potential function and the negated gradient is defined as follows,

$$U_{rep}(q) = \frac{1}{2}\eta\left(\frac{1}{\rho(q)} - \frac{1}{\rho_0}\right) \tag{14}$$

$$-\nabla U_{rep}(q) = \left(\frac{1}{\rho(q)} - \frac{1}{\rho_0}\right)\frac{1}{\rho^2(q)}\frac{q - q_c}{\left\|q - q_c\right\|} \tag{15}$$

ρ_0 is the distance of influence and q_c is the configuration at which the object is closest to the obstacle. The repulsive potential and the total potential are presented in Figure 7 and Figure 8, respectively.

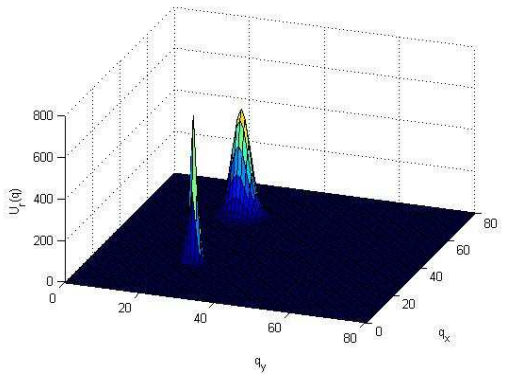

Figure 7 Repulsive potential function $U_{rep}(q)$ for two obstacles

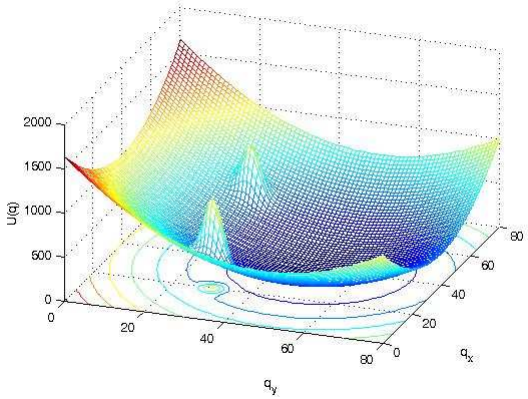

Figure 8 Total potential function U(q)

Beginning from an initial configuration, gradient descent attempts to find a configuration at which $\nabla U(q_i)$ becomes zero – the goal. Because this condition cannot be satisfied exactly, ε is chosen so that $\| \nabla U(q_i) \| < \varepsilon$ [4].

The potential field method is fast but has the local minimum problem. To compensate this problem random sampling methods suggest a solution.

3.3 Kinodynamic Motion Planning

The kinodynamic motion planning is a probabilistic method and suggests a solution for the above-mentioned local minimum problem of the potential field method. In kinodynamic motion planning, dynamic constraints as well as the kinematic constraints are considered. Because of the difficulty to represent kinodynamic constraints in the configuration space *C*, a new space – the state space *S* – is introduced [12]. The state space consists of the configuration and the information of the velocity of the moving object. Accordingly, the purpose of kinodynamic motion planning is the determination of a path that fulfills both the requirements of generating a *collision-free* path as well as *satisfying* kinodynamic constraints.

Kinematic constraints (e.g. configuration for avoiding obstacles) accounts for the relationship between the configuration *q* and the velocity of the moving object and can be expressed as follows,

$$F(q, \dot{q}) = 0 \tag{16}$$

These constraints can be classified into *holonomic* and *non-holonomic* constraints [4,13,17,18]. Holonomic constraints implies that the velocity of the object has not to be considered (e.g. $F(q) = 0$) while non-holonomic constraints indicates that the integration of the velocity is not possible. The criterion of non-holonomic constraints is given in [13].

Furthermore, the dynamic constraint should be considered as well. In addition to the configuration and the velocity of the moving object, the dynamic constraint involves also the acceleration of this object.

If path planning methods focus solely on kinematic constraints, it is plausible that significant dynamic aspect of the motion of the moving object cannot be reflected properly [16,17,18]. Thus, kinematic and dynamic constraints both have to be regarded in searching an *admissible path* for a moving object.

If the control inputs are regarded as well, then we can broaden our scope of consideration to the *control system* [12]. The control system represents the relationship between the *object's state* $s \in S$ and the *control inputs* $u \in \Omega$ - where S and Ω represent the *state space* and *control space*, respectively - and can be described as follows,

$$\dot{s} = f(s, u) \tag{17}$$

With these definitions, the motion planning for objects – i.e. robot, UAV - amidst moving obstacles under compliance with kinodynamic constraints can be achieved by *sampling-based algorithms*. The sampling-based algorithm does not show the complexity such as the roadmap method in finding a path as the dimension of the configuration space grows [4,12]. The cardinal aspect of sampling-based algorithms is to generate samples being *collision-free* configurations of the moving object and to connect the generated samples so that a path can be found. The sampling-based algorithm can further be classified into the *multi-query planning* and the *single-query planning* [12]. The advantage of the single-query planning compared to the multi-query planning is that no pre-computation of the roadmap or environment has to be carried out. As a result, the single-query planning is appropriate for path planning in *fast-changing* environment. An example for this single-query planning is the RRT (Rapidly-exploring Random Tree).

As the name implies, the RRT builds incrementally a tree in the state space that finally connects q_{init} and q_{goal}. Assume that for any situation, the robot's equation of motion and the control function are known. Starting from q_{init}, a random configuration q_{rand} is selected by means of uniform distribution. In the next step, the nearest vertex to q_{rand} is found and is denoted as q_{near}. Applying a control input u for incremental small time δt, a new configuration q_{new} which is on the line from q_{near} to q_{rand} can be derived. After that step, it has to be controlled whether a collision with an obstacle occurs during this step. If there is no collision, then q_{new} is added to the tree as a new vertex and the edge q_{near} - q_{new} is added to the tree as well. This iteration continues until the tree approaches q_{goal} sufficiently close. The scheme is presented in Figure 9.

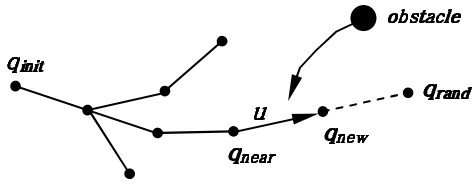

Figure 9 Scheme of RRT

The RRT is to a high degree fast in the generation of feasible path and it works reliable in high dimension state spaces [10]. Accordingly, practical applications are introduced in [2,7,10,16].

In addition to the presented RRT, advanced methods like goal-biased RRT – which search for q_{rand} toward the goal – and bidirectional RRT – where the tree is built from q_{init} as well as from

q_{goal} – can be applied.

Furthermore, [4] suggest a variable step size and thus a variable time δt in dependency of the distance between the object and obstacles.

3.4 Measurement Unit

Unlike the range measuring devices for mobile robots or conventional airplane, the sensors for small UAVs are restricted in their weights and sizes. Therefore, the major aspect in implementing an appropriate sensor for the UAV will be the compact size and less weight at approximate equivalent performance.

In this regard, in [2] the implementation of an appropriate Laser Range Finder and its application is introduced. This category of Laser Range Finder with a data rate of 10 Hz at a weight of approximate 230 g has a maximum measuring distance of 730 m. Because the weight requirement including all other units – e.g. telemetry, control and navigation unit etc. – for the developed UAV of the Technische Universität Braunschweig should not exceed 5 kg, our finding in proper Laser Range Finder will be concentrated to the above-mentioned category. The Laser Range Finder shall provide information about range, velocity and the relative direction of obstacle to the UAV.

A further challenge in implementing a Laser Range Finder will be the ability of this sensor to scan a two-dimensional field so that the UAV is provided with a kind of map of the terrain with potential obstacles.

Accordingly, further investigation in finding and implementing the sensor to the UAV shall be done parallel to the application of the path planning algorithms.

4. Summary and Outlook

An integrated navigation system based on a tightly-coupled GPS/INS integration architecture was developed. The filter uses range and carrier phase measurements from a stand-alone single-frequency GPS receiver to aid the INS. In order to avoid solving for the integer ambiguity but to profit from the high measurement accuracy of the carrier phase, time-differenced carrier phase were used. Flight tests were carried out with the institutes GN&C test platform (UAV). It was shown that the MEMS-based navigation system achieves an attitude accuracy (1σ) of about 0.6° in pitch and roll, and 1.1° in yaw.

Besides the GPS-INS integration, this paper presented methods with which an UAV is able to navigate autonomously in unexplored environments. The potential field method seems to be auspicious for generating path except for the local minimum problem. For the solution of local minimum problem, however, heuristic method can be applied so that configurations about the local minimum are selected randomly. The kinodynamic motion planning is another approach to generate a path without being trapped in a local minimum. This method seems to be appropriate in generating feasible paths for the UAV. Therefore, further research will be focused on the implementation of these mentioned path planning methods parallel to the experiments with sensors such as Laser Range Finder.

Reference

1 Amato, N.: Randomized Motion Planning: Techniques and Applications, 2004

2 Beard, R., Saunders, J.B.: Static and Dynamic Obstacle Avoidance in Miniature Air Vehicles, AIAA 2005-6950, 2005

3 Beard, R., McClain, T.: Motion Planning Using Potential Fields, BYU 2003

4 Choset, H. et al.: Principles of Robot Motion, MIT Press, 2005

5 Donald, B., Xavier, P.: Kinodynamic Motion Planning, Journal of the Association for Computing Machinery, Vol. 40, No.5, pp.1048-1066, 1993

6. Farrell, J.L.: Carrier Phase Processing Without Inte-gers. In: Proceedings of the Institute of Navigation 57th Annual Meeting (Albuquerque, NM, June 11-13, 2001), pp. 423-428

7 Frazzoli, E., Dahleh, M.A., Feron, E.: Real Time Motion Planning for Agile Autonomous Vehicles, Journal of Guidance, Control, and Dynamics, Vol. 25, No.1, 2002

8. Gelb, A.: Applied Optimal Estimation. 11th Printing. Cambridge, MA, London : The M.I.T. Press, 1989

9. van Graas, F. ; Farrell, J.L.: GPS/INS – A Very Dif-ferent Way. In: Proceedings of the Institute of Navigation 57th Annual Meeting (Albuquerque, NM, June 11-13, 2001), pp. 715-721

10 Kim, J., Ostrowski, J.P.: Motion Planning of Aerial Robot using Rapidly-exploring Random Trees with Dynamic Constraints, IEEE International Conference on Robotics and Automation, Taipei, Taiwan, September 2003

11 Langelaan, J., Rock, S.: Navigation of Small UAVs Operating in Forests, 2004-5140, 2004

12 Latombe, J.C., Hsu, D.: Motion Planning: Recent Developments

13 Latombe, J. C.: Robot Motion Planning, Kluwer Academic Publishers, 1991

14 LaValle, S.M.: Planning Algorithms, Cambridge University Press, 2006

15 LaValle, S.M.: From Dynamic Programming to RRTs: Algorithmic Design of Feasible Trajectories, Control Problems in Robotics, pp.19-37, Springer Verlag, Berlin, 2002

16 LaValle, S.M., Cheng, P., Shen, Z.: RRT-Based Trajectory Design for Autonomous Automobiles and Spacecraft, Archives of Control Sciences, Vol. 11, No.3-4, pp.51-78, 2001

17 LaValle, S.M., Kuffner, J.: Rapidly-Exploring Random Trees: Progress and Prospects, Workshop on the Algorithmic Foundations of Robotics, 2000

18 LaValle, S.M., Kuffner, J.: Randomized Kinodynamic Planning, IEEE International Conference on Robotics and Automation, pp. 473-479, 1999

19. Schulz, H.-W. ; Buschmann, M. ; Kordes, T. ; Krüger, L. ; Winkler. S. ; Vörsmann, P.: The Autonomous Micro and Mini UAVs of the Carolo-Family In: Proceedings of the AIAA Infotech@Aerospace (Arlington, Virginia, Sep. 26-29, 2005, AIAA-2005-7092

20 Tolg, B.: Entwicklung einer Simulationsumgebung zur Trajetorienplanung für mobile Roboter, 2001

21. Wendel, J. ; Obert, T. ; Trommer, G.F.: Enhancement of a Tightly Coupled GPS/INS System for High-Precision Attitude Determination of Land Vehicles. In: Proceedings of the Institute of Navigation 59th Annual Meeting/CIGTF 22nd Guidance Test Sym-posium (Albuquerque, NM, June 23-25, 2001), pp. 200-208

22. Winkler, S. ; Schulz, H.-W. ; Buschmann, M. ; Vörsmann, P.: Testing GPS/INS Integration for Autonomous Mini and Micro Aerial Vehicles. In: Proceedings of the ION GNSS 2005 (Long Beach, CA, Sep. 13-16, 2005)

23 Zhao, Y.J.: Trajectory Planning for Autonomous Aerospace Vehicles amid Known Obstacles and Conflicts, Journal of Guidance, Control, and Dynamics, Vol. 27, No.6, 2004